

Part-per-million gas detection from long-baseline THz spectroscopy

S. A. Harmon and R. A. Cheville^{a)}

School of Electrical and Computer Engineering, Oklahoma State University, Stillwater, Oklahoma 74078

(Received 10 May 2004; accepted 6 July 2004)

We report a long-baseline THz time domain spectrometer based on a White cell design capable of detecting gas species in the low part-per-million range in near real time. Coherent transients from methyl chloride vapor are observed directly in the time domain using a 5.0 m path length at pressures down to 1 Pa. Both phase sensitive (lock-in) detection and direct signal averaging using a rapid-scanning delay line are used for data acquisition. © 2004 American Institute of Physics. [DOI: 10.1063/1.1788896]

Optically generated pulses of electromagnetic radiation with terahertz (THz) bandwidths are used for spectroscopic characterization of a wide variety of material systems. By measuring a picosecond duration electromagnetic pulse after propagation through a sample and an identical length of free space, THz time domain spectroscopy (THz-TDS)¹ determines the absorption and dispersion of a sample over a broad frequency spectrum. THz-TDS has been used for characterization of semiconductors and dielectrics,¹ liquids,² and gas samples.^{3,4} In liquid and solid samples rapid dephasing gives rise to broad features with widths of tens to hundreds of cm^{-1} due to absorption by free carriers, optical phonons, or rapid collision-induced reorientation of molecular dipole moments.

In contrast to condensed matter, the complex permittivity of gases at THz frequencies arises from rotational transitions between well-defined states in isolated molecules. Since collision times are typically on the order of hundreds of picoseconds to nanoseconds, distinct spectral lines are measured with widths of a fraction of an inverse cm at atmospheric pressure. Since $\Delta\nu \ll \nu_0$, and the spectrum of THz-TDS measurements covers over a decade in frequency, the simultaneous measurement of many lines or species is possible. The nearly single-cycle THz pulse excites the manifold of rotational transitions, creating a coherent ensemble that reradiates pulses via free-induction decay (FID).⁴ The FID is the time-domain analog of the frequency-domain spectral response, and permits the identification of molecular species by their time domain response rather than their spectral signature. The individual spectral lines combine to give an aggregate time signature while spectral line broadening is observed directly as the coherence relaxation, or collisional dephasing, time.⁴

Previous work on THz gas sensing has demonstrated detection of multiple species at down to 307 Pa ($7.2 \times 10^{16} \text{ cm}^{-3}$) using linear predictive coding.⁵ Also gas filter correlation spectroscopy has detected 30 part-per-million (ppm) of H_2S at STP ($7.3 \times 10^{14} \text{ cm}^{-3}$).⁶ Here we demonstrate detection of gas species number densities corresponding to the low part-per-million range by THz-TDS using a THz White cell to achieve a variable path length from 2.5 to 7.5 m. For a path length of 5.0 m, it is possible to directly identify methyl chloride by the location of the FID echo at pressures of 1 Pa ($2.4 \times 10^{14} \text{ cm}^{-3}$).

The THz-TDS system used for these measurements is adapted from time-domain spectrometers reported previously,¹ shown in Fig. 1. The THz pulse is generated by a photoconductively switched coplanar stripline on semi-insulating GaAs, which is collimated by a Si lens and off-axis parabolic mirror. The THz pulse is detected by an optically gated 50 μm dipole antenna fabricated on ion-implanted silicon-on-sapphire. To achieve detection of low number densities, the optical path length is extended from tens of centimeters to over 5 m using a White cell⁷ configuration shown in Fig. 1.

The THz White cell is contained in a Vacuum chamber with a base pressure of less than 0.2 Pa. Both high resistivity silicon ($n=3.42$) and high-density polyethylene (HDPE) windows are used for coupling the THz beam into the vacuum chamber. Compared to HDPE, silicon windows are lossless across the pulse bandwidth, but result in a 51% amplitude reflection loss of the THz pulse due to Fresnel reflections. The other terahertz optics, including the transmitter and receiver, are outside the vacuum chamber, as shown in Fig. 1, in an airtight enclosure purged with dry air containing approximately 250 ppm H_2O vapor. After evacuating the vacuum chamber to the base pressure, the THz White cell is filled with methyl chloride gas to a desired pressure using a mass flow controller. Pressure is measured to an accuracy of ± 0.1 pa using a convection gauge; water vapor partial pres-

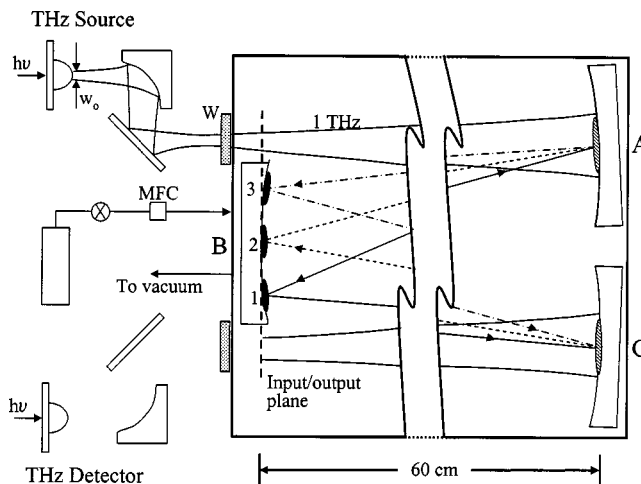


FIG. 1. Experimental setup depicting the THz white cell, and external THz optics. The spot sizes on mirrors A, B, and C are shown approximately to scale for a frequency of 1 THz.

^{a)} Author to whom correspondence should be addressed; electronic mail: kridnix@okstate.edu

sure is monitored using a hygrometer accurate to a number density better than $2.7 \times 10^{13} \text{ cm}^{-3}$. The accuracy of the measurements is determined by system drift; to ensure data accuracy, a reference THz pulse was measured with the cell under vacuum both before and after each measurement.

A White cell acts as a unity conjugate ratio imaging system, with an object located at the input plane to the cell forming an image at the output plane (dashed line in Fig. 1). First surface aluminum-coated spherical mirrors with a 15 cm aperture and 30 cm focal length, separated by twice their focal length, were used as the primary optics of the cell since they have near-unity reflectance at THz frequencies. The number of passes (four, eight or twelve single passes) is controlled by the angles of mirrors A and C, corresponding to path length of 2.5, 5.0, or 7.5 m. A similar White cell is used on the optical gating beam to maintain synchronization between the optical and THz pulses.

Due to diffraction of the millimeter and submillimeter THz wavelengths, the spatial extent of the THz beam on mirror B and the size of the THz beam on mirrors A and C limit the achievable path length. The THz beam maintains a constant position on mirrors A and C where the beam diameter is largest while the beam strikes a different point on mirror B on each pass. While a larger beam size at the cell image plane minimizes diffraction, resulting in a smaller spot size on mirrors A and C, the low frequency response of the system is reduced due to clipping of the low frequencies (larger spot sizes) on mirror B. Conversely, a small input spot size at the entrance plane will result in rapid expansion of the THz beam due to diffraction with commensurately large spot sizes and clipping of the low frequencies on mirrors A and C. Figure 1 shows the THz beam approximately to scale for a frequency of 1 THz. Using Gaussian beam formalism,⁸ the beam diameter at 1 THz is calculated to be 41 and 20 mm on mirrors A and B, respectively.

Since the THz measurement system is phase coherent, optimal power transfer requires that the THz beam exiting the White cell have an identical phase and amplitude profile to the beam entering.⁹ This is not possible in a White cell without the use of external beam correction optics, which are not utilized in the configuration shown. For the White cell configuration of Fig. 1 the calculated power coupling efficiency to the THz detector—based on the assumption of a $\text{TEM}_{0,0}$ mode with initial waist of 2.5 mm—is approximately 12% integrated over the measured system bandwidth of 0.1–1.8 THz. Since the coherent measurement system detects the time-varying electric field of the THz pulse, the detected signal is proportional to the square root of the power transfer, or 35% of an optimal system. Design consideration of the THz White cell, including beam-forming optics, will be discussed in a subsequent publication.

The THz pulse transmitted through the evacuated THz White cell with a 5 m path length is shown in Fig. 2(a). The system spectral bandwidth, obtained by a numerical Fourier transform, is shown in the upper inset. The sharp spectral features are due to absorption by residual water vapor in the THz beam path, seen as oscillations following the THz pulse, expanded in the lower inset. After methyl chloride is added to the cell to a total pressure of 1 mbar, the measured THz pulse is shown in Fig. 2(b). The reshaped and attenuated excitation pulse is followed by a series of coherent transients,^{3,4} which decay because of collisional dephasing. The large amplitude of the sixth coherent transient is an ex-

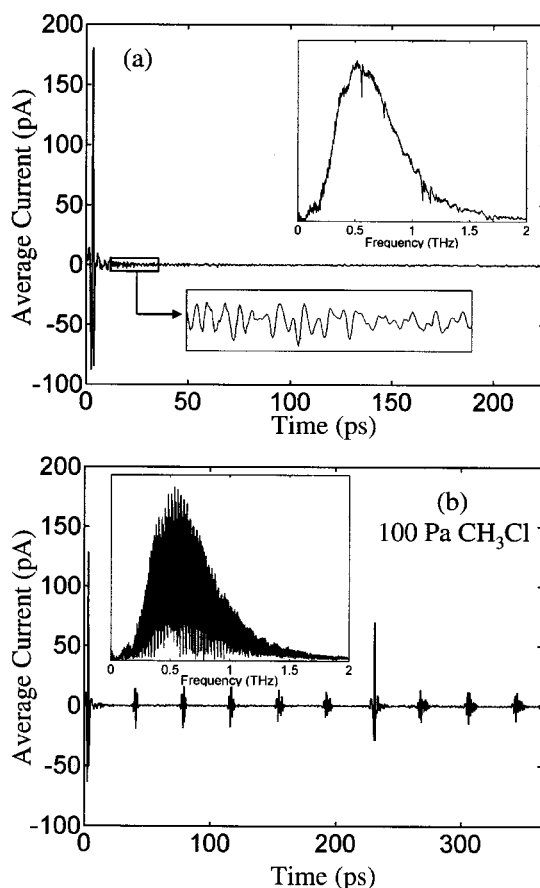


FIG. 2. (a) THz reference pulse for evacuated cell. Lower inset is time response of residual water vapor. The spectral response of the system is shown in the upper inset; spectral features result from residual water vapor. (b) Reshaped THz pulse and subsequent train of coherent transients with 100 Pa of methyl chloride.

perimental artifact arising from reflections within the high resistivity silicon window. The inset to Fig. 2(b) shows the THz spectrum corresponding to methyl chloride which appears nearly solid due to the 0.013 THz spacing of the rotational absorption lines.

Coherent transients are seen in all symmetric molecules with a permanent dipole moment. Molecules which are not symmetric, H_2O for example [Fig. 2(a)], have a more complex time domain structure. At the low pressures measured here, the time between collisions is¹⁰

$$\frac{1}{\tau} = \sum N_i \sigma \sqrt{\frac{8kT}{\pi M_i}},$$

where N is the number density, M the mass, $\sigma = 4.13 \times 10^{-15} \text{ cm}^2$ is the collisional cross section of methyl chloride,¹¹ and the sum is done over the two major Cl isotopes of CH_3Cl . At 100 Pa the collisional dephasing time is approximately 284 ns ($\Delta\nu = 1.1 \text{ MHz}$), nearly three orders of magnitude longer than the temporal extent of the data. The reshaping of the coherent transients in Fig. 2(b) with increasing time is due to deviation from the rigid-rotator-model,¹⁰ lifting of the degeneracies for the K quantum number resulting in a K dependent line shift,³ and the two naturally occurring isotopes of chlorine, Cl^{35} and Cl^{37} .

For symmetric molecules such as CH_3Cl , monitoring a specific temporal location for the presence of a particular echo of the free induction decay allows near real-time gas

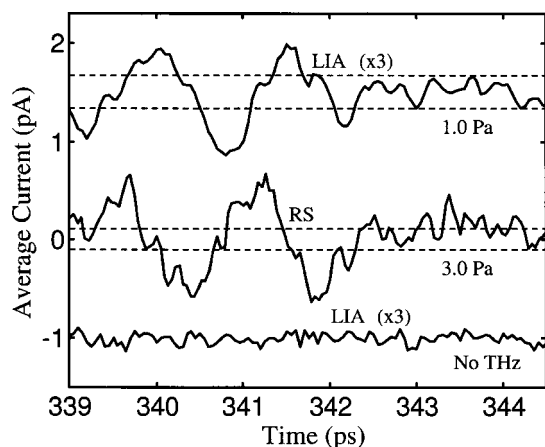


FIG. 3. The ninth coherent echo measured using lock-in amplification (LIA) and rapid scanning (RS) techniques. Scans acquired using LIA have been multiplied by a factor of 3 for clarity. The dashed lines are the rms values of the respective scans. The lower curve gives the baseline noise level detected with no THz pulse using LIA detection.

detection, illustrated in Fig. 3. Here real-time signal averaging is used over a 5 ps window at 340 ps from the main pulse to detect the ninth coherent echo. The upper trace in Fig. 3 was performed using a lock-in amplifier (LIA) for 1 Pa of methyl chloride, and has been expanded by a factor of 3 for clarity. This measurement was obtained in approximately 8.5 min with a 1 s time constant. Using a rapid scanning (RS) delay line, the middle scan in Fig. 3 was acquired by averaging 5000 scans in 3.5 min (1500 scans per min) at a pressure of 3 Pa of methyl chloride. For both of these methods, an averaged reference scan was subtracted in order to eliminate the empty cell baseline caused by residual water vapor [Fig. 2(a)]. The dashed lines overlaying the two upper measurements of Fig. 3 represent the rms values of the reference scan. The residual water vapor is the major factor affecting the baseline noise as illustrated by the lower curve in Fig. 3 which shows the baseline noise level with no THz

pulse. The difference in temporal position between the ninth echo between the LIA and RS techniques is due to temperature fluctuations that occurred during the course of the LIA measurement resulting in slight changes in the nonresonant index of air and/or thermal expansion of the White cell. Over the 5 m length of the THz White cell a 0.25 ps shift corresponds to a change in optical path length—either Δn or Δd —of 7.5×10^{-5} , which can be achieved by less than a 1°C change in ambient temperature.

We have demonstrated detection in near real-time of polar molecules in the time domain using THz time domain spectroscopy. The detection limit can be further reduced by increasing the path length of the THz White cell and increasing the coupling efficiency of the system.

The authors would like to acknowledge support from the National Science Foundation (ECS-9984896), Army Research Office (DAAD19-99-R-BAA8), and Department of Energy.

¹D. Grischkowsky, S. Keiding, M. van Exter, and Ch. Fattinger, *J. Opt. Soc. Am. B* **7**, 2006 (1990).

²J. T. Kindt and C. A. Schmuttenmaer, *J. Phys. Chem.* **100**, 10373 (1996).

³H. Harde, R. A. Cheville, and D. Grischkowsky, *J. Phys. Chem. A* **101**, 3646 (1997).

⁴H. Harde, S. Keiding, and D. Grischkowsky, *Phys. Rev. Lett.* **66**, 1834 (1991).

⁵R. H. Jacobsen, D. M. Mittleman, and M. C. Nuss, *Opt. Lett.* **21**, 2011 (1996).

⁶G. Mouret, W. Chen, G. Boucher, R. Bocquet, P. Mounaix, and D. Lipens, *Opt. Lett.* **24**, 351 (1998).

⁷J. U. White and S. O. D. C. Esso Laboratories, *J. Opt. Soc. Am.* **32**, 285 (1942).

⁸M. T. Reiten, S. A. Harmon, and R. A. Cheville, *J. Opt. Soc. Am. B* **20**, 2215 (2003).

⁹J. C. G. LeSurf, *Millimeter-wave Optics, Devices, and Systems* (Adam Hilger, Bristol, 1990).

¹⁰C. H. Townes and A. L. Schawlow, *Microwave Spectroscopy* (Dover, New York, 1975).

¹¹L. Frenkel, S. J. Kryder, and A. A. Maryott, *J. Chem. Phys.* **44**, 2610 (1996).